Innovative Ti/Fe/Eu-Carbon composite for Cephalexin adsorption

Compósito innovador de Ti/Fe/Eu-Carbón para la adsorción de cefalexina

Gómez-Vilchis, J.C.*[a], García-Rosales, G.*[b], Lóngoria-Gándara, L.C.[c] and Tenorio-Castilleros, D.[d]

[a] ROR Tecnológico Nacional de México – Instituto Tecnológico de Toluca• LKK-0328-2024 • 0000-0002-1023-9651 • 957883

[b] ROR Tecnológico Nacional de México – Instituto Tecnológico de Toluca • LKK-5096-6657 • 0000-0003-4438-6657 • 43369

[c] ROR International Atomic Energy Agency • 0000-0001-8524-9777

[d] ROR Instituto Nacional de Investigaciones Nucleares• 0000-0001-7742-2437 • 5288
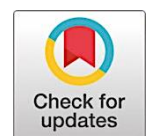
Abstract

The study focused on developing an innovative material for the adsorption of antibiotics in contaminated water. A biochar modified with titanium (Ti), iron (Fe), and europium (Eu) (Ti/Fe/Eu-Carbon) was synthesized to adsorb cephalexin (CEX) from aqueous solutions. The biochar was characterized using techniques such as SEM, EDS, and XPS, which confirmed the presence and energy states of Ti, Fe, and Eu. The material exhibited an impressive specific surface area of 232 m² g⁻¹ and a mesoporous structure. Adsorption experiments revealed that CEX adsorption occurs through both physisorption and chemisorption, achieving a maximum adsorption capacity of 600 µg g⁻¹, compared to 90 µg g⁻¹ for unmodified biochar. Optimal adsorption conditions were identified at pH 7 and a temperature of 20°C, as the process was found to be exothermic and spontaneous. Furthermore, the material demonstrated reusability for up to eight cycles.

Resumen

El estudio se centró en el desarrollo de un material innovador para la adsorción de antibióticos en aguas contaminadas. Se sintetizó un biocarbón modificado con titanio (Ti), hierro (Fe) y europio (Eu) (Ti/Fe/Eu-Carbón) para adsorber cefalexina (CEX) de soluciones acuosas. El biocarbón fue caracterizado mediante técnicas como SEM, EDS y XPS, las cuales confirmaron la presencia y los estados energéticos de Ti, Fe y Eu. El material mostró una notable área superficial específica de 232 m² g⁻¹ y una estructura mesoporosa. Los experimentos de adsorción revelaron que la adsorción de CEX ocurre a través de procesos de fisisorción y químisorción, alcanzando una capacidad máxima de adsorción de 600 µg g⁻¹, en comparación con los 90 µg g⁻¹ del biocarbón no modificado. Las condiciones óptimas de adsorción se identificaron a pH 7 y a una temperatura de 20°C, ya que el proceso resultó ser exotérmico y espontáneo. Además, el material demostró ser reutilizable hasta en ocho ciclos.

Adsorption, Composite, cephalexin.

Adsorción, Compósito, Cefalexina

Journal of Systematic Innovation   8[22]1-16: e2822116

Article

Introduction

In recent years, the use of antibiotics has increased significantly, leading to their presence as pollutants in rivers (Su et al., 2023), groundwater, lakes, wastewater (Durán-Álvarez et al., 2023), and, in some cases, drinking water (Wang et al., 2023). Excessive use of antibiotics results in the emergence of resistant bacteria (Jampani et al., 2024), and these substances can also be persistent, bioaccumulative, and toxic in the environment (Li et al., 2023).

Despite their environmental impact, antibiotics are crucial for treating a wide range of infections caused by both Gram-negative and Gram-positive bacteria (Ali et al., 2023). Among the most used antibiotics is cephalexin, a β-lactam derivative (Gou et al., 2021) used to treat urinary tract infections, respiratory tract infections, and other common bacterial infections (Bailey et al., 1970).

Due to their presence in wastewater effluents, new methods are sought for their removal, including membrane bioreactors, phytoremediation, photodegradation, and adsorption, among others. However, adsorption has been extensively studied due to its ease of operation, low cost, and reusability.

Among, the most efficient adsorbent materials are composites, which are matrices loaded with particles that enhance their physical and chemical properties (Wang et al., 2022). This is due to significant increases in surface area, stability, resistance, and thermal conductivity. Chemically modified biocarbons are used as composites, particularly those loaded with metal oxides and salts.

For example, the presence of iron (Fe_2O_4) and titanium (TiO_2) oxides has been reported to facilitate the formation of oxygen-rich functional groups, leading to the creation of mesopores and an increased surface area (Liang et al., 2024; Nakarmi et al., 2022; Guo et al., 2022).

Lanthanide-based compounds have gained popularity in recent years due to their stability across various pH ranges and excellent chemical stability (Kajjumba et al., 2022).

The presence of metal and lanthanide oxides has shown favorable results, as demonstrated by Gong et al. (2024), because they enhance pollutant retention through functional groups on the surface, improving adsorption capacity.

Additionally, these compounds, when supported in small amounts on biocarbon, can achieve up to 98% efficiency due to the formation of active sites on the surface (Lan et al., 2022) which create new oxygen vacancies (Lin et al., 2018), particularly with europium due to its oxidation states (2^+ or 3^+).

Due to their physical and chemical properties, binary and ternary metal oxide systems attract significant attention as potential agents for removing emerging contaminants (Lǚ et al., 2013).

Consequently, metal and lanthanide oxide particles supported on biocarbon present a promising material for cephalexin removal due to their efficiency and low production cost.

In this study, a composite with Ti, Fe, Eu particles supported on biocarbon was synthesized for the removal of cephalexin in aqueous phase, evaluating the effects of various parameters such as time, initial concentration, pH, and temperature. Its ease of preparation, combined with its versatility, offers significant advantages for future use in treating antibiotic-contaminated waters.

Methodology

Materials

To prepare the composite, preconditioned avocado pits were used along with the following reagents: HNO_3 (J.T Baker®, 70%), NaOH (Fermont®), C_2H_6O (J.T Baker®, 99%), Ti[OCH(CH₃)₂]₄ (Sigma-Aldrich®, 97%), Fe(NO₃)₃ · 9H₂O (Sigma-Aldrich®, 98%), Eu(NO₃)₃ · 5H₂O (Sigma-Aldrich®) and a Cephalexin standard (1000 mg L⁻¹) (Sigma-Aldrich®), from which the solutions were prepared.

Preparation of Ti/Fe/Eu-Carbon composite

The avocado seeds were repeatedly washed with distilled water to remove impurities and then dried at room temperature for 72 h.

The dried seeds were ground and sieved to obtain a particle size of 0.83 mm. The powdered material was washed several times with hot water and then dried at 40°C for 24 h.

To prepare the composite, 10 mL of C_2H_6O was added to a reactor and stirred continuously at 30°C. Gradually, 350 µL of a $Ti[OCH(CH_3)_2]_4$ solution was added dropwise. The mixture was stirred for 15 min at 70°C, after which 10 mL each of $Fe(NO_3)_3 \cdot 9H_2O$ and $Eu(NO_3)_3 \cdot 5H_2O$ solutions (0.03 M) were added.

Finally, 3 grams of avocado seed powder were introduced into the reactor, which was then sealed and placed in a temperature-controlled shaking bath at 50°C for 12 h. After the reaction, the impregnated material was pyrolyzed at 650°C for 3 h. The resulting composite was named Ti/Eu/Fe-Carbon.

Morphological and Surface Characterization

To analyze the morphology of the material, a JEOL® JSM-5900 LV scanning electron microscope was used, equipped with an OXFORD® INCAx-Act 51-ADD0013 probe for elemental analysis. This analysis was conducted across five different areas.

The isoelectric point (IP) of the material was determined by placing 0.005, 0.05, 0.1, 0.15, 0.25, 0.35, 0.45, 0.55, and 1 g of the material into polypropylene tubes, each containing 10 mL of deionized water at 25°C. The tubes were stirred continuously for 24 h. The pH was then measured in each tube using a HANNA Instruments® potentiometer, and the data were plotted.

To determine the specific surface area, pore volume, and average pore size of the composite, a Belsorp Max III instrument was used in a nitrogen environment. The sample underwent a degassing pretreatment for 2 h at 200°C using a Belpre II instrument. The density of active sites was assessed following the methodology reported by Hayes et al., (1991).

Energy state analysis was performed using the Thermo Scientific K-Alpha X-Ray Photoelectron Spectrometer®, equipped with an Al (Kα) X-ray source. The instrument conducted 10 scans per sample in normal lens mode, with an aperture size of 400 µm and a step size energy of 0.030 eV.

Adsorption Experiments

To assess the adsorption capacity of CEX for the composite, kinetic and adsorption isotherm experiments were also conducted with carbon without Ti/Fe/Eu, to use it as a blank (BC) and evaluate its contribution to the process. A 500 µg L^{-1} solution of CEX was used, and the experiments were carried out using batch methodology, with CEX residues quantified using a Perkin Elmer® Lambda 35 UV-Vis spectrophotometer at $\lambda = 250$ nm.

The CEX adsorption kinetics were studied using polyethylene tubes with 1 mg of material each and 5 mL of a CEX solution at 200 µg L^{-1}. Experiments were conducted at different contact times: 5, 10, 30 min, 1, 2, 3, 6, 9, 12, 15, 18, and 24 h. The tubes were agitated in a temperature-controlled shaking bath at 20, 30, and 40 °C and pH=7. The data obtained were fitted to the Lagergren, Ho-Mackay, and Elovich mathematical models.

For the adsorption isotherms, the same conditions were used with different CEX concentrations (150, 160, 170, 180, 190, 200, 220, and 240 µg L^{-1}), with agitation for 24 h at 20, 30, and 40 °C and pH = 7. The data obtained were fitted to the Langmuir, Freundlich, and Temkin mathematical models.

The adsorption capacity q_e (µg g^{-1}) was calculated using Equation 1.

$$q_e = \frac{(C_0 - C_e)\,V}{M} \qquad [1]$$

Where C_0 (µg L^{-1}) (µg L^{-1}) is the initial concentration, and C_e is the equilibrium concentration; M (g) is the weight of the adsorbent material, and V (L) is the volume of the solution.

On the other hand, to evaluate the adsorption capacity of the materials as a function of pH, polypropylene tubes were used. Each tube contained 1 mg of material and 5 mL of the CEX solution. The initial pH was adjusted by adding small volumes of HNO_3 and/or NaOH (0.1 M).

The experiments were conducted across a pH range of 2 to 12 at 20, 30, and 40 °C, with continuous agitation for 24 h. Afterward, each tube was centrifuged at 2500 rpm for 3 min and the concentration was determined using UV-vis spectroscopy.

Gómez-Vilchis, J.C., García-Rosales, G., Lóngoria-Gándara, L.C. and Tenorio-Castilleros, D. [2024]. Innovative Ti/Fe/Eu-Carbon composite for Cephalexin adsorption. Journal of Systematic Innovation. 8[22]1-16: e2822116.
https://doi.org/10.35429/JSI.2024.8.22.1.16

To determine reuse cycles, regeneration tests were conducted by subjecting the adsorbent material to a desorption process for 1 h in an acidic medium (pH=2) using 0.1 M HNO₃. Subsequently, 1 mg of each material was reintroduced into a contaminant solution at 20 °C and pH = 7, and this procedure was repeated until the minimum adsorption percentages were achieved.

Results

Characterization

The characterization of the composite, presented in Fig. 1a, shows a structure with semicircular cavities approximately 40 µm in diameter, whose rough walls may facilitate the diffusion of contaminants within the material. This type of structure is relevant for applications where accessibility and distribution of the contaminant within the material are crucial, as the cavities can serve as sites for accumulation and adsorption.

Within these cavities, as shown in Fig. 1b, there are small spherical particles with an average diameter of 1.8 ± 0.3 µm, forming clusters (Fig. 1c) with an elemental composition of C (77.82%), O (19.55%), Ti (0.89%), Fe (0.84%), and Eu (0.90%). These particles correspond to the titanium, iron, and europium oxides formed in the composite. The presence of these particles is consistent with findings reported by Fazal et al. (2020) and Viglašová et al. (2020), who observed similar morphologies in metal oxide compounds.

This validates that the synthesis method used produces a material with the expected morphology and functionality for adsorption applications. Fig. 1d shows the effect of the CEX adsorption process on the Ti/Eu/Fe-Carbon composite. While the general morphology remains similar, deformation in the cavities is observed, with tighter folds in the walls. This deformation may result from the adsorption process, which could induce structural changes in the material. However, the persistence of the spherical particles ((C (82.36%), O (16.38%), Ti (0.35%), Fe (0.48%), and Eu (0.43%)) indicates that, despite the morphological changes, the fundamental characteristics of the composite remain intact.

Regarding the elemental composition, the carbon (C) percentage increases from 77.82% to 82.36% after adsorption, while the percentages of oxygen (O), titanium (Ti), iron (Fe), and europium (Eu) decrease. The increase in carbon content may be attributed to the adsorption of CEX on the material's surface, which raises the proportion of carbon in the elemental analysis. The decrease in other elements may reflect the specific interaction between the material and the contaminant, altering the relative proportions of the detected elements. This is consistent with findings by Nawas et al. (2023), which suggest that interactions between the material and the contaminant can alter the observed elemental composition.

Box 1
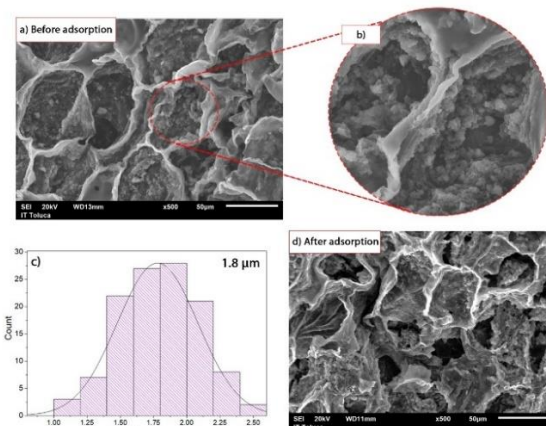
Figure 1

a) Micrograph of Ti/Eu/Fe-Carbon; b) Formation of spherical particles; c) Particle size distribution; d) Post-adsorption of CEX

The specific surface area of Ti/Eu/Fe-Carbon, which is 232 m²/g, exceeds that reported for other biochars modified with iron and lanthanide oxides, as noted in the studies by Fan et al. (2021) and Yaghini & Faghihian (2020). A similar value is reported by Wang et al. (2023).

This increase in surface area can be attributed to the presence of metal oxide particles in the material, which enhance the surface area due to increased dispersion and the formation of a more porous structure.

Ti/Eu/Fe-Carbon is classified as mesoporous, with a pore diameter of 2.69 nm. According to IUPAC definitions, mesoporous materials have pore sizes ranging from 2 to 50 nm (Mangeli et al., 2021). Additionally, the material has a pore volume of 0.1565 cm³ g⁻¹.

The presence of mesopores in the material is beneficial for adsorption, as it facilitates greater contact between the material's surface and contaminants, promoting better diffusion of these contaminants to the active surface.

The number of active sites, calculated from the specific surface area, is 20 sites nm^{-2}, indicating a high density of available sites for adsorption. This value is crucial for assessing the material's capacity to capture and retain contaminants.

The isoelectric point (IP) of Ti/Eu/Fe-Carbon was determined to be at a pH of 8. This pH is where the material's charges are in equilibrium, meaning the material has no net charge. An IP of 8 is consistent with values reported for some biochars (D'Cruz et al., 2020). Below this pH, the material's surface charge is positive due to an excess of [H$^+$] ions, while above this pH, the charge is negative due to an excess of [OH$^-$] ions.

These results are similar to those reported by Chen et al. (2023) in a ternary Fe-Ca-La compound and Cheng et al. (2023) in a Ca-Al-La compound.

These findings are promising for the adsorption of CEX, as the chemical speciation of CEX varies with pH, which can influence its adsorption capacity on the material (Watanabe et al., 2010). The well-defined IP and high specific surface area make Ti/Eu/Fe-Carbon an effective candidate for adsorption applications, as it can adapt to pH changes and provide high adsorption capacity due to its mesoporous structure and high density of active sites.

Adsorption experiments

In Fig. 2a, the comparison between Ti/Eu/Fe-Carbon and white Carbon (BC) shows a significant increase in adsorption capacity, rising from 90 to 560 μg L^{-1}. This substantial improvement suggests that the addition of Ti/Eu/Fe greatly enhances the adsorption efficiency of BC. This positive effect can be attributed to the presence of metal oxides, which appear to enhance the material's adsorptive properties. Fig. 2b presents the kinetic data for CEX adsorption onto the materials.

The maximum adsorption capacity is achieved at 560 μg L^{-1} at 20 °C. Adsorption efficiency is high from the first minutes of contact but decreases over time until equilibrium is reached in 1 h. This behavior is due to the progressive reduction in active sites (H$^+$, OH$^-$) on the materials and the decreasing concentration of CEX in the solution.

The decrease in the adsorption rate over time indicates that the active sites become saturated with CEX molecules, leading to an equilibrium state (Mishra et al., 2023). This behavior is comparable to that observed in the adsorption of pharmaceuticals such as venlafaxine, trazodone, and fluoxetine using eucalyptus-derived biochar (Puga et al., 2022).

The high initial adsorption rate is consistent with findings by Lu & Zhao (2024), who reported similar results using biochar derived from fish scales and pine needles for ciprofloxacin adsorption.

It is also observed that the adsorption capacity decreases with increasing temperature, suggesting that the adsorption process is exothermic. This phenomenon may be explained by the ability of CEX molecules to gain sufficient thermal energy to overcome the activation barrier and bind more effectively to the biochar surface, enhancing the adsorbent-adsorbate interaction (Azeez et al., 2024). Additionally, when CEX penetrates the internal pores of the biochars, these pores may become blocked, reducing the number of CEX molecules that can access the material.

To determine the influence of the initial concentration of CEX on the adsorption process and to identify the optimal time for maximizing the amount of adsorbed contaminant, adsorption isotherms are used. These isotherms allow for the evaluation of the adsorbents' capacity and performance by fitting experimental values to established mathematical models and comparing these models. Fig. 2c shows the behavior of CEX adsorption isotherms on the biochars, with adsorption capacities ranging from 600, 540, to 475 μg g^{-1}.

The decrease in adsorption capacity with increasing temperature may be attributed to CEX molecules having sufficient thermal energy to overcome the activation barrier and bind more effectively to the biochar surface, favoring the adsorbent-adsorbate interaction.

Gómez-Vilchis, J.C., García-Rosales, G., Lóngoria-Gándara, L.C. and Tenorio-Castilleros, D. [2024]. Innovative Ti/Fe/Eu-Carbon composite for Cephalexin adsorption. Journal of Systematic Innovation. 8[22]1-16: e2822116.
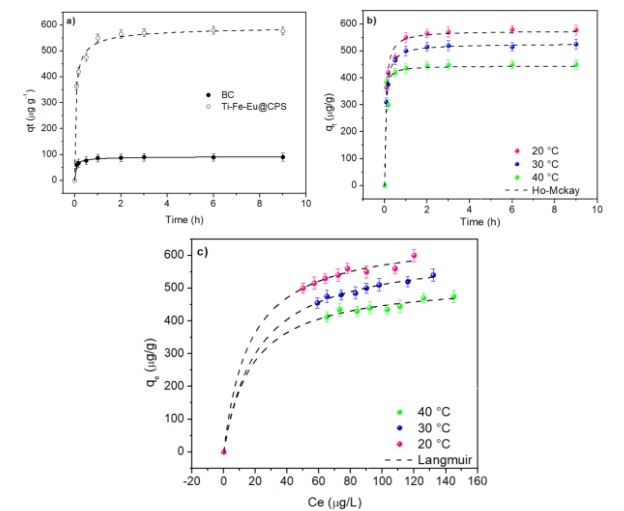https://doi.org/10.35429/JSI.2024.8.22.1.16

Box 2

Figure 2

a) Comparison of BC vs. Ti/Eu/Fe-Carbon b) kinetics and a) adsorption isotherms of CEX on Ti/Eu/Fe-Carbon at 20, 30 and 40 °C.

The kinetic adsorption data for CEX (Table 1) were fitted to various kinetic adsorption models (Lagergren, Ho-Mackay, and Elovich), with the best fit obtained using the Ho-Mackay model (Eq. 2), showing a correlation coefficient of 0.99-0.98 Ti/Eu/Fe-Carbon.

This suggests that in the CEX adsorption process, the reaction rate depends on the amount of solute adsorbed onto the adsorbent surface and the amount adsorbed at equilibrium (Ho et al., 1999).

This implies that the adsorption process is chemical in nature. These findings are consistent with the results reported by Wernke et al. (2020), who investigated CEX adsorption using graphene oxide, and Naghipour et al. (2019), who used a biocarbon derived from banana wood.

$$q_t = \frac{K_2 q_e^2 t}{1 + K_2 q_e t} \qquad [2]$$

Where q_e (mg g^{-1}), represents the adsorption capacity at equilibrium, and q_t (mg g^{-1}) represents the amount of solute adsorbed at time t (Oyekanmi et al., 2024).

Box 3

Table 1

Fitting of mathematical models for the adsorption kinetics of CEX on Ti/Eu/Fe-Carbon

T (°C)		20	30	40
Pseudo first order	$K_L (min^{-1})$	1597.1	1453.2	267.6
	q_e $(\mu g\ g^{-1})$	512.8	465.6	416.7
	R^2	0.8	0.7	0.8
Pseudo second order	K $(g\ \mu g^{-1}$ $min^{-1})$	0.03	0.05	0.08
	q_e $(\mu g\ g^{-1})$	575	527	444.4
	R^2	**0.98**	**0.99**	**0.98**
Elovich	$A\ (\mu g$ $g^{-1}min^{-1})$	5.90E+04	4.14E+04	3.98E+04
	$B\ (g\ \mu g^{-1})$	0.09	0.08	0.06
	R^2	0.98	0.98	0.97

The results of fitting the adsorption isotherms to the Langmuir, Freundlich, and Temkin mathematical models, presented in Table 2, indicate that the Langmuir model (Eq. 3) provides the best fit for the experimental data. Based on these findings and the XPS analysis, the proposed adsorption mechanism suggests that the adsorption of CEX onto Ti/Eu/Fe-Carbon involves both chemisorption and physisorption processes. In this mechanism, CEX molecules form chemical bonds with the adsorbent surface while also interacting through electrostatic forces (Moreroa-Monyelo et al., 2022).

The Langmuir model assumes that adsorption occurs at specific and homogeneous sites on the adsorbent surface, with each site accommodating only one molecule of adsorbate. The dimensionless parameter R$_L$, calculated as R$_L$ = 1/(1 + K$_L$Co), is used to interpret the nature of the adsorption process: R$_L$>1 indicates unfavorable adsorption: R$_L$=1 adsorption is linear; R$_L$<1 the adsorption is favorable and R = 0 the adsorption is irreversible.

In this study, the R$_L$ values are less than 1, demonstrating that the adsorption of CEX on Ti/Eu/Fe-Carbon is favorable. This indicates a strong affinity of the CEX molecule for the material's surface, facilitating its adsorption.

This finding supports the notion that chemisorption is the predominant mechanism in the interaction between CEX and the adsorbent.

Gómez-Vilchis, J.C., García-Rosales, G., Lóngoria-Gándara, L.C. and Tenorio-Castilleros, D. [2024]. Innovative Ti/Fe/Eu-Carbon composite for Cephalexin adsorption. Journal of Systematic Innovation. 8[22]1-16: e2822116.
https://doi.org/10.35429/JSI.2024.8.22.1.16

$$q = \frac{q_0 y}{K_d + y} \qquad [3]$$

Where: q_0 is the maximum adsorption capacity of the adsorbent, K_d is the equilibrium constant, y is the concentration of solute in the solution, and q is the amount of solute adsorbed per unit of adsorbent (Fan et al., 2021).

Box 4
Table 2

Fitting of kinetic adsorption models for CEX on Ti/Eu/Fe-Carbon

T (°C)		20	30	40
Langmuir	q_m ($\mu g\ g^{-1}$)	892.7	883.4	878.8
	K_L ($L\ \mu^{-1}$)	-1.82 E+45	-4.56 E+44	-1.72 E+44
	R_L	-2.5E-48	-9.9E-48	-2.6E-47
	R^2	**0.99**	**0.99**	**0.98**
Freundlich	K_F ($\mu g\ g^{-1}$) ($L\ \mu g^{-1}$)$^{1/n}$	447.3	385.1	265.3
	n	0.37	0.39	0.53
	R^2	0.95	0.97	0.97
Temkin	q_m ($\mu g\ g^{-1}$)	7.17	6.24	5.41
	K_T ($\mu g\ L^{-1}$)	2.25	1.7	0.77
	R^2	0.93	0.92	0.95

In Table 3, the maximum sorption capacities (q_m) of CEX at different temperatures are compared with those reported in other studies. It is important to note that while the experimental conditions used vary, comparing q_m values remains valid as it provides insight into the performance of Ti/Eu/Fe-Carbon relative to other materials.

Some studies report higher adsorption capacities than those observed in this research. However, it is crucial to consider that many of these studies use larger amounts of adsorbent material for their adsorption experiments. In contrast, the advantage of the Ti/Eu/Fe-Carbon material lies in the fact that only 1 mg of adsorbent is used.

This suggests that despite the smaller amount of material, Ti/Eu/Fe-Carbon demonstrates a competitive or superior performance in adsorption capacity compared to other materials that require more adsorbent.

Box 5
Table 3

Comparison of CEX adsorption capacity in Ti/Eu/Fe-Carbon with literature values

Adsorbents	Adsorption capacity (q_m)	Co	Mass (mg)	Reference
Graphene oxide	164 mg g^{-1}	100	10	Wernke et al., 2020
Actived carbón	48 mg g^{-1}	50	-	Rashtbari et al., 2018
Bauxita	112 mg g^{-1}	300	10	Giannoulia et al., 2024
Biochar	57 mg g^{-1}	20	30	Acelas et al., 2021
Graphene	650 mg g^{-1}	700	-	Ali et al., 2023
Ti/Eu/Fe-Carbon	600 $\mu g\ g^{-1}$	0.2	1	This work

Impact of temperature on CEX adsorption onto Ti/Eu/Fe-Carbon

The study involved testing at different temperatures (20, 30, and 40 °C) to assess how temperature affects the adsorption process of CEX on Ti/Eu/Fe-Carbon. Temperature is a crucial factor in adsorption processes, as it can influence various properties of both the adsorbent and the adsorbate.

Firstly, temperature can impact the deprotonation of functional groups on the adsorbent's surface. This can lead to an increase in the concentration of hydroxyl groups (OH^-) on the surface, potentially altering the material's adsorption capacity. An increase in OH^- groups might enhance the interaction between the adsorbent and the adsorbate, depending on the nature of the chemical interactions involved (Masulli et al., 2022).

Additionally, temperature affects the kinetic energy of the adsorbate molecules and their solubility in the solution. Higher temperatures increase the mobility of the molecules, facilitating their diffusion to the adsorbent's surface. This effect can improve the adsorption process's efficiency by allowing greater mass transfer (Wong et al., 2008).

An increase in temperature can also influence the reaction rate of the adsorption process. Chemical reactions typically accelerate with rising temperature due to increased kinetic energy, which can impact the reaction rate constant.

Gómez-Vilchis, J.C., García-Rosales, G., Lóngoria-Gándara, L.C. and Tenorio-Castilleros, D. [2024]. Innovative Ti/Fe/Eu-Carbon composite for Cephalexin adsorption. Journal of Systematic Innovation. 8[22]1-16: e2822116.
https://doi.org/10.35429/JSI.2024.8.22.1.16

In aqueous solutions, temperature can affect the amount of dissolved molecular oxygen, which in turn can impact reactions involving oxygen (Karlsson et al., 2017; Groeneveld et al., 2023).

To quantify the effect of temperature on the adsorption rate, kinetic data were collected at the three mentioned temperatures and an Arrhenius plot was constructed. The plot was developed by plotting the natural logarithm of the rate constant (Ln k) against 1/T (K). The linearized form of the Arrhenius equation, shown in equation 5, allows for the calculation of activation energy and evaluation of how temperature affects the adsorption reaction rate (Eq. 5).

$$Lnk = \frac{Ea}{R}\left(\frac{1}{T}\right) + LnA \qquad [4]$$

Where k is the rate constant for the reaction at a given temperature, Ea is the activation energy for the process, R is the gas constant (8.314 kJ (mol·K)$^{-1}$), T is the temperature in Kelvin, and AAA is the frequency factor for the reaction.

As shown in Table 4, the thermodynamic parameters indicate that an increase in temperature reduces the interaction between the materials and the CEX molecule. The values for ΔH°, ΔS°, and ΔG° were determined using the equations provided (Eq. 5 and 6).

$$\Delta G° = \Delta H° - T\Delta S° \qquad [5]$$

$$Ln\ k = -\frac{\Delta°H}{R} * \frac{1}{T°} + \frac{\Delta S°}{R} \qquad [6]$$

Box 6

Table 4

Thermodynamic parameters obtained

T	Thermodynamic parameters			
(°C)	Ea (kJ mol^{-1})	ΔG° (kJ mol^{-1})	ΔH° (kJ mol^{-1})	ΔS° (J mol K^{-1})
20		-46.30	-19.75	-0.09
30	8.75E^{-05}	-47.20		
40		-48.11		

The activation energy (Ea) for CEX adsorption being greater than 40 kJ mol^{-1} suggests that the process involves chemisorption (Acelas et al., 2021).

This indicates that the adsorption is driven by strong chemical interactions between the adsorbate and the adsorbent. The negative values for ΔH° and ΔS° point to an increase in disorder at the liquid-solid interface and confirm that the adsorption process is exothermic.

This implies that the adsorption process releases heat and is accompanied by a decrease in the system's entropy (Imanipoor et al., 2020). As temperature increases, the binding potential at equilibrium decreases, leading to a reduction in sorption capacity (Gao et al., 2020). This trend aligns with the exothermic nature of the adsorption process, where higher temperatures can diminish the adsorbent's ability to bind the adsorbate effectively. Conversely, the negative values of ΔG° indicate a decrease in Gibbs free energy, demonstrating that the adsorption process is thermodynamically favorable and feasible through chemical interactions between the adsorbate and adsorbent (Kaya et al., 2024).

However, Fakhri et al. (2014) observed that an increase in temperature reduces CEX adsorption on carbonaceous materials, attributing this decrease to the exothermic nature of the process. This reduction can be explained by the weakening of Van der Waals forces between CEX molecules and the adsorbent material at higher temperatures (Wernke et al., 2020).

Effect of pH and adsorption mechanism of CEX on Ti/Eu/Fe-Carbon

In Fig. 3a, the data reveal that as pH increases, the percentage of CEX adsorbed rises up to pH 7, after which it starts to decline. This trend highlights the significant impact of pH on CEX adsorption efficiency. CEX exists in different ionic forms depending on the pH: cationic below pH 3, zwitterionic between pH 3 and 7, and anionic above pH 7 (Watanabe et al., 2010).

The increased adsorption observed between pH 5 and 7 aligns with the zwitterionic form of CEX, which has both positive and negative charges that interact favorably with the adsorbent surface.

The isoelectric point (IP) of the adsorbent material is 8. At pH levels below this IP, the adsorbent surface is positively charged, attracting the anionic forms of CEX.

However, at pH levels lower than 3, the cationic form of CEX and the positively charged adsorbent create electrostatic repulsion, which reduces adsorption efficiency.

The significant adsorption at pH 5, consistent with findings from Rashtbari et al. (2020), supports the notion that the zwitterionic form of CEX shows a higher affinity for the adsorbent. This optimal pH range enhances the interaction between zwitterionic CEX and the adsorbent material. Between pH 4 and 6, increased adsorption is likely due to chemisorption, as indicated by previous kinetic studies.

At these pH levels, the zwitterionic CEX facilitates stronger chemical interactions with the adsorbent, leading to enhanced adsorption.

Beyond pH 7, where CEX becomes anionic, reduced adsorption is attributed to repulsion between the negatively charged CEX and the similarly charged or neutral adsorbent surface, leading to decreased interaction and adsorption efficiency. In summary, the adsorption of CEX is primarily influenced by its ionic form and the surface charge of the adsorbent material.

The data suggest that zwitterionic CEX, prevalent between pH 5 and 7, interacts most effectively with the adsorbent, thereby enhancing chemisorption and overall adsorption efficiency (Fig. 3b).
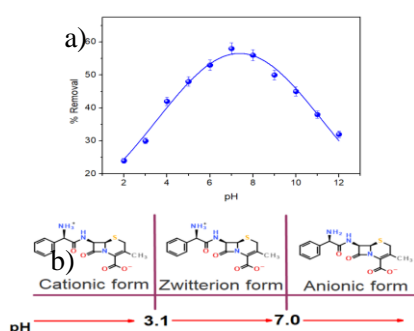
Box 7

Figure 3

Effect of pH on the adsorption of CEX onto Ti/Eu/Fe-Carbon; b) Ionic species of CEX

In the context of cefalexin adsorption, X-ray photoelectron spectroscopy (XPS) has proven to be an essential tool for elucidating the energetic states on the surface of the Ti/Eu/Fe-Carbon material.

The XPS analysis identified various energetic states within the material's components, including C1s, O1s, N1s, Ti2p, Fe2p, and Eu3d, offering a detailed view of the chemical interactions relevant to cefalexin adsorption. In the C1s spectrum, with a full width at half maximum (FWHM) of 1.1 ± 0.1, several bands were observed, corresponding to different energetic states including $C=C$ (aromatic), C-N, C-O, and $C=O$ (carboxyl groups) (Fig. 4a) (Choi et al., 2019; Peng et al., 2017). These functional groups are crucial for interacting with cefalexin, as they can form specific bonds with the antibiotic, thereby enhancing its adsorption on the material's surface.

The O1s spectrum, with an FWHM of 1.4 ± 0.1, revealed energetic states associated with O-Metal, $O=C$, O-C, and $O-C=O$ (Suo et al., 2021; Dodevski et al., 2017) (Fig. 4b). These oxygen states may play a key role in forming electrostatic interactions and hydrogen bonds with cefalexin, which could significantly influence its adsorption capacity. In the N1s spectrum, with an FWHM of 1.4 ± 0.1 (Fig. 4c), specific energetic states such as N-C and $N=C$ were detected, related to pyridinic and pyrrolic nitrogen forms (Lawrie et al., 2007; Chen et al., 2014).

The presence of nitrogen could affect cefalexin adsorption through coordination bonds or acid-base interactions. The Ti2p analysis identified peaks corresponding to Ti^{4+} and Ti^{3+} at 464, 460, and 458 eV, respectively, indicating the presence of TiO_2 in the material (Kramar et al., 2024). The formation of TiO_2 could impact the material's adsorption capacity by modifying the surface and its reactivity (Fig. 4d).

In the Fe2p spectrum, peaks corresponding to Fe^{2+} at 709 eV and Fe^{3+} at 710.3 eV were detected (Rivera et al., 2020) (Fig. 4e). The oxidation states of iron may influence cefalexin interactions, potentially through ionic or redox mechanisms. Finally, the Eu3d spectrum showed two primary peaks at 1134.8 eV (Eu^{3+} 3d5/2) and 1126.2 eV (Eu^{2+} 3d5/2), along with two smaller satellite peaks at 1164.1 eV (Eu^{3+} 3d5/2) and 1155.5 eV (Eu^{2+} 3d3/2) (Brunckova et al., 2021) (Fig. 4f)

The presence of europium may impact the material's stability and its ability to adsorb cefalexin.

Gómez-Vilchis, J.C., García-Rosales, G., Lóngoria-Gándara, L.C. and Tenorio-Castilleros, D. [2024]. Innovative Ti/Fe/Eu-Carbon composite for Cephalexin adsorption. Journal of Systematic Innovation. 8[22]1-16: e2822116.
https://doi.org/10.35429/JSI.2024.8.22.1.16

In summary, XPS analysis provides a comprehensive understanding of the oxidation states and chemical interactions on the surface of the Ti/Eu/Fe-Carbon material. This detailed insight is crucial for optimizing the material's performance in cefalexin adsorption and other related processes.

Box 8
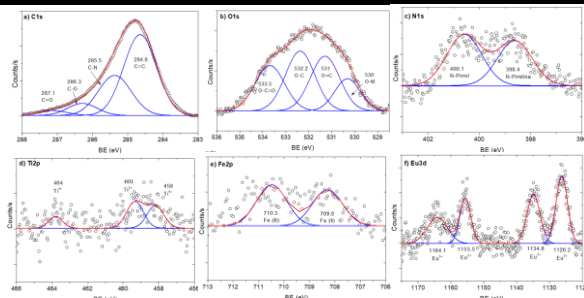
Figure 4

Deconvolution of a) C1s, b) O1s, c) N1s, d) Ti2p, e) Fe2p, and f) Eu3d

The proposed interaction mechanism between cefalexin (CEX) and the Ti/Eu/Fe-Carbon composite, illustrated in Figure 5 and supported by characterization results, adsorption isotherms, kinetic studies, and XPS data, offers a detailed understanding of the adsorption process.

The Ti/Eu/Fe-Carbon composite contains Ti, Fe, and Eu ions, which significantly contribute to CEX adsorption through electrostatic attractions. At pH 7, CEX exists in its dipolar form, possessing both positive and negative charges. The predominant oxidation states of titanium (Ti^{4+}, Ti^{3+}), iron (Fe^{2+}, Fe^{3+}), and europium (Eu^{3+}, Eu^{2+}) interact with water to form active sites such as OH^- and H^+. These sites exhibit a high affinity for the charges on the CEX molecule, promoting adsorption. For example, OH^- groups on the material can interact with the amino groups (NH_3^+) in CEX, facilitating the adsorption process (Cao et al., 2021).

Active H^+ sites on the material's surface can form hydrogen bonds with the oxygen atoms in the CEX molecule. Conversely, the amine groups in CEX can donate H^+ and form hydrogen bonds with the OH^- groups on the material's surface, a process known as hydrogen bonding (Ndoun et al., 2021). This interaction stabilizes CEX on the material's surface, enhancing adsorption.

The presence of aromatic rings in CEX is also crucial for adsorption capacity. The hexagonal structure of these rings facilitates adsorption onto carbon-based materials, with antibiotics having more aromatic rings adsorbing more rapidly due to π-π interactions (Acelas et al., 2021).

Additionally, hydrophobic C-C interactions are observed, where the methyl group in CEX interacts with methyl groups in Ti/Eu/Fe-Carbon. These interactions are driven by the hydrophobic nature of the involved groups (Krasucka et al., 2021). Furthermore, covalent C-O bonds are formed between the methyl group of CEX and the active OH^- sites on the material, further stabilizing and enhancing the adsorption process.

Based on our observations, the interaction mechanisms between CEX and the Ti/Eu/Fe-Carbon composite involve a combination of electrostatic attractions, hydrogen bonding, π-π interactions, hydrophobic interactions, and covalent bonding. Each of these mechanisms plays a crucial role in optimizing the adsorption of CEX onto the composite material, underscoring the importance of understanding and leveraging these interactions for effective adsorption.

Box 9
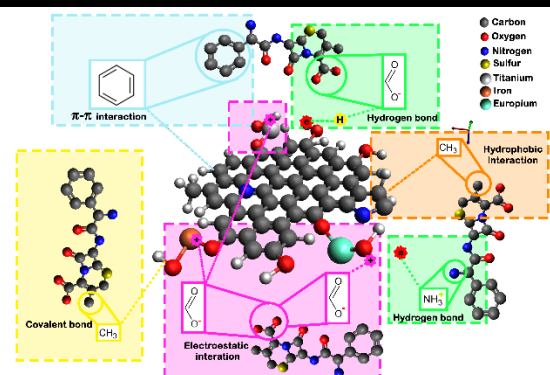
Figure 5

Mechanism of adsorption of CEX on Ti/Eu/Fe-Carbon

Reusability

Figure 6 depicts the percentage removal of cefalexin (CEX) by Ti/Eu/Fe-Carbon, which is used to assess the material's reuse and stability, crucial for evaluating its cost-effectiveness. For CEX desorption, an acidic solution with pH = 2 was employed since, at this pH, CEX is in its cationic form, which reduces its adsorption capacity.

Gómez-Vilchis, J.C., García-Rosales, G., Lóngoria-Gándara, L.C. and Tenorio-Castilleros, D. [2024]. Innovative Ti/Fe/Eu-Carbon composite for Cephalexin adsorption. Journal of Systematic Innovation. 8[22]1-16: e2822116.
https://doi.org/10.35429/JSI.2024.8.22.1.16

Journal of Systematic Innovation

Article

The results reveal a decline in removal efficiency with each cycle of adsorption-desorption. Specifically, after 8 cycles, the removal efficiency decreased from 77% to 17% at 20°C, from 74% to 13% at 30°C, and from 70% to 12% at 40°C.

This performance drop indicates that the Ti/Eu/Fe-Carbon composite loses effectiveness over multiple cycles. Several factors might contribute to this decrease.

Repeated usage may deplete the active sites on the material, diminishing its adsorption capacity. Additionally, the acidic desorption environment and varying temperatures could affect the composite's structural integrity, further compromising its performance.

The substantial reduction in removal efficiency suggests that while Ti/Eu/Fe-Carbon may initially perform well, its long-term usability could be limited.

For practical applications, it is essential to address these issues and consider methods for regenerating or improving the material's stability to enhance its economic viability.
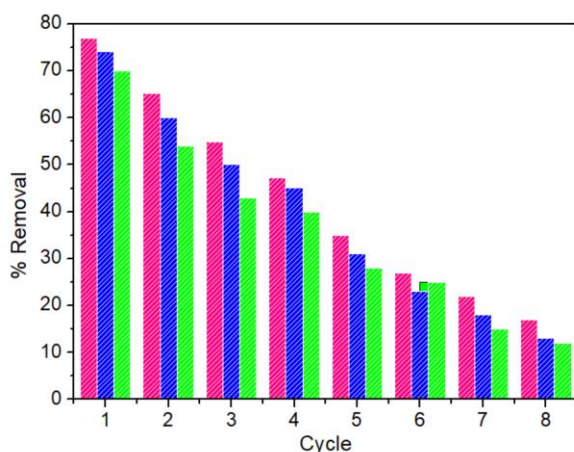
Box 10

Figure 6

Reusability cycles at 20, 30 and 40 °C of Ti/Eu/Fe-Carbon

Conclusions

The Ti/Eu/Fe-Carbon composite synthesized from avocado seeds presents a promising solution for addressing antibiotic contamination in water, specifically targeting cefalexin (CEX). This study highlights its effectiveness in removing CEX, achieving a notable removal efficiency of 80% ($160\,\mu g\,L^{-1}$).

The composite's performance is optimized under specific conditions at 20°C, a pH of 7, and a contact time of 1 h demonstrating its efficiency and stability. The material's ability to be reused up to 8 times underscores its practical applicability and economic viability in water treatment processes.

The fitting of adsorption isotherms to the Langmuir, Freundlich, and Temkin mathematical models, as shown in Table 2, indicates that the Langmuir model (Eq. 3) provides the best fit for the experimental data. Based on these results and XPS analysis, the proposed interaction mechanism suggests that the adsorption of CEX onto Ti/Eu/Fe-Carbon involves both chemisorption and physisorption processes. In this mechanism, CEX molecules form chemical bonds with the adsorbent surface while also interacting through electrostatic forces (Moreroa-Monyelo et al., 2022).

Thermodynamic analysis reveals that the process is exothermic, with decreasing efficiency at higher temperatures, suggesting that the composite performs better in cooler conditions. This characteristic can be advantageous in specific environmental contexts or treatment scenarios.

Overall, this study underscores the potential of Ti/Eu/Fe-Carbon derived from avocado seeds as an innovative and effective material for mitigating antibiotic pollution. Its combination of high removal efficiency, reusability, and favorable adsorption properties makes it a valuable addition to the field of water treatment, offering a sustainable approach to combatting emerging environmental contaminants.

Declarations

Conflict of interest

The authors declare no conflicts of interest. They have no known financial or personal relationships that could have influenced the content of this article.

Author contribution

Gómez-Vilchis, J. C.: Conducted the experiments, analyzed and interpreted the data, and wrote the paper.

Gómez-Vilchis, J.C., García-Rosales, G., Lóngoria-Gándara, L.C. and Tenorio-Castilleros, D. [2024]. Innovative Ti/Fe/Eu-Carbon composite for Cephalexin adsorption. Journal of Systematic Innovation. 8[22]1-16: e2822116.
https://doi.org/10.35429/JSI.2024.8.22.1.16

Article

García-Rosales, G.: Designed and conceptualized the experiments, analyzed and interpreted the data, provided reagents, materials, analysis tools, or data, and contributed to writing and editing the article.

Longoria-Gándara, L. C.: Analyzed and interpreted the data and wrote the paper.

Tenorio-Castilleros, D.: Assisted with the analysis of several samples.

Availability of data and materials

The data are available and can be requested from the corresponding author.

Abbreviations

BC	Blank biochar
C	Carbon
CEX	Cephalexin
Ea	Activation energy
EDS	Energy Dispersive Spectroscopy
Eu	Europium
Fe	Iron
FWHM	The Full Width Half Maximum
G°	Gibbs free energy
H°	Enthalpy
IP	Isoelectric Point
N	Nitrogen
O	Oxygen
S°	Entropy
SEM	Scanning Electron Microscopy
Ti	Titanium
UV-Vis	UV-Visible Spectrophotometry
XPS	X-Ray Photoelectron Spectroscopy

References

Antecedents

Gong, W., Qi, C., Huang, L., Tian, Z., Huang, Z., Tao, C., Lin, H., Guo, L., & Yu, Z. (2024). Adsorption of phosphorus in wastewater by lanthanum-modified magnetic sewage sludge biochar. *Desalination and Water Treatment*, *320*, 100603.

Guo, D., Feng, D., Zhang, Y., Zhang, Z., Wu, J., Zhao, Y., & Sun, S. (2022). Synergistic mechanism of biochar-nano TiO_2 adsorption-photocatalytic oxidation of toluene. *Fuel Processing Technology*, *229*, 107200.

Liang, H., Zhu, C., Wang, A., & Chen, F. (2024). Facile preparation of $NiFe_2O_4$/biochar composite adsorbent for efficient adsorption removal of antibiotics in water. *Carbon Research*, *3*(1), 2.

Nakarmi, K. J., Daneshvar, E., Eshaq, G., Puro, L., Maiti, A., Nidheesh, P. V., Wang, H., & Bhatnagar, A. (2022). Synthesis of biochar from iron-free and iron-containing microalgal biomass for the removal of pharmaceuticals from water. *Environmental Research*, *214*, 114041.

Wang, G., Li, Y., Dai, J., & Deng, N. (2022). Highly efficient photocatalytic oxidation of antibiotic ciprofloxacin using TiO_2@g-C_3N_4@biochar composite. *Environmental Science and Pollution Research*, *29*(32), 48522-48538.

Basics

Azeez, L., Adefunke, O., Oyedeji, A. O., Agbaogun, B. K., Busari, H. K., Adejumo, A. L., Agbaje, W. B., Adeleke, A. E., & Samuel, A. O. (2024). Facile removal of rhodamine B and metronidazole with mesoporous biochar prepared from palm tree biomass: adsorption studies, reusability, and mechanisms. *Water Practice & Technology*, *19*(3), 730-744.

Bailey, A., Hadley, A., Walker, A., & James, D. G. (1970). Cephalexin a new oral antibiotic. *Postgraduate Medical Journal*, *46*(533), 157-158.

Brunckova, H., Mudra, E., Rocha, L., Nassar, E., Nascimento, W., Kolev, H., Kovalcikova, A., Molcanova, Z., Podobova, M., & Medvecky, L. (2021). Preparation and characterization of isostructural lanthanide Eu/Gd/Tb metal-organic framework thin films for luminescent applications. *Applied Surface Science, 542,* 148731.

Cao, Y., Xie, X., Tong, X., Feng, D., Lv, J., Chen, Y., & Song, Q. (2021). The activation mechanism of Fe(II) ion-modified cassiterite surface to promote salicylhydroxamic acid adsorption. *Minerals Engineering, 160,* 106707.

Chen, S., Cao, Y., & Feng, J. (2014). Polydopamine As an Efficient and Robust Platform to Functionalize Carbon Fiber for High-Performance Polymer Composites. *ACS Applied Materials & Interfaces, 6*(1), 349–356.

Choi, S. W., Tang, J., Pol, V. G., & Lee, K. B. (2019). Pollen-derived porous carbon by KOH activation: Effect of physicochemical structure on CO_2 adsorption. *Journal of CO_2 Utilization, 29,* 146–155.

Dodevski, V., Janković, B., Stojmenović, M., Krstić, S., Popović, J., Pagnacco, M. C., Popović, M., & Pašalić, S. (2017). Plane tree seed biomass used for preparation of activated carbons (AC) derived from pyrolysis. Modeling the activation process. *Colloids and Surfaces A: Physicochemical and Engineering Aspects, 522,* 83–96.

Durán-Álvarez, J. C., Prado, B., Zanella, R., Rodríguez, M., & Díaz, S. (2023). Wastewater surveillance of pharmaceuticals during the COVID-19 pandemic in Mexico City and the Mezquital Valley: A comprehensive environmental risk assessment. *Science of The Total Environment, 900,* 165886.

Gou, Y., Peng, L., Xu, H., Li, S., Liu, C., Wu, X., Song, S., Yang, C., Song, K., & Xu, Y. (2021). Insights into the degradation mechanisms and pathways of cephalexin during homogeneous and heterogeneous photo-Fenton processes. *Chemosphere, 285,* 131417.

Hayes, K. F., Redden, G., Ela, W., & Leckie, J. O. (1991). Surface complexation models: An evaluation of model parameter estimation using FITEQL and oxide mineral titration data. *Journal of Colloid and Interface Science, 142*(2), 448-469.

Ho, Y. S., & McKay, G. (1999). Pseudo-second order model for sorption processes. *Process Biochemistry, 34*(5), 451-465.

Jampani, M., Mateo-Sagasta, J., Chandrasekar, A., Fatta-Kassinos, D., Graham, D. W., Gothwal, R., Moodley, A., Chadag, V. M., Wiberg, D., & Langan, S. (2024). Fate and transport modelling for evaluating antibiotic resistance in aquatic environments: Current knowledge and research priorities. *Journal of Hazardous Materials, 461,* 132527.

Kajjumba, G. W., & Marti, E. J. (2022). A review of the application of cerium and lanthanum in phosphorus removal during wastewater treatment: Characteristics, mechanism, and recovery. *Chemosphere, 309,* 136462.

Kramar, A., Bibik, Y., Dyachenko, A., Chernyayeva, O., Vorobets, V., Kolbasov, G., Smirnova, N., Gaidai, S., Ischenko, O., Eremenko, A., & Linnik, O. (2024). Advanced design of sol-gel derived multilayered cerium titanate films: structural, surface, photoelectrochemical and photocatalytic properties. *Materials Chemistry and Physics, 324,* 129679.

Lan, Y., Gai, S., Cheng, K., Li, J., & Yang, F. (2022). Lanthanum carbonate hydroxide/magnetite nanoparticles functionalized porous biochar for phosphate adsorption and recovery: Advanced capacity and mechanisms study. *Environmental Research, 214,* 113783.

Lawrie, G., Keen, I., Drew, B., Chandler-Temple, A., Rintoul, L., Fredericks, P., & Grøndahl, L. (2007). Interactions between Alginate and Chitosan Biopolymers Characterized Using FTIR and XPS. *Biomacromolecules, 8*(8), 2533–2541.

Li, X., & Cheng, H. (2023). Mn-modified biochars for efficient adsorption and degradation of cephalexin: Insight into the enhanced redox reactivity. *Water Research, 243,* 120368.

Lin, X., Chen, H., Hu, Z., Hou, Y., & Dai, W. (2018). Enhanced visible light photocatalysis of TiO2 by Co-modification with Eu and Au nanoparticles. *Solid State Sciences, 83,* 181–187.

Lǚ, J., Liu, H., Liu, R., Zhao, X., Sun, L., & Qu, J. (2013). Adsorptive removal of phosphate by a nanostructured Fe–Al–Mn trimetal oxide adsorbent. *Powder Technology*, *233*, 146–154.

Mishra, A., Ojha, H., Pandey, J., Tiwari, A. K., & Pathak, M. (2023). Adsorption characteristics of magnetized biochar derived from Citrus limetta peels. *Heliyon*, *9*(10), e20665.

Oyekanmi, A. A., Katibi, K. K., Omar, R. C., Ahmad, A., Elbidi, M., Alshammari, M. B., & Shitu, I. G. (2024). A novel oil palm frond magnetic biochar for the efficient adsorption of crystal violet and sunset yellow dyes from aqueous solution: synthesis, kinetics, isotherm, mechanism and reusability studies. *Applied Water Science*, *14*(2), 13.

Peng, H., Gao, P., Chu, G., Pan, B., Peng, J., & Xing, B. (2017). Enhanced adsorption of Cu(II) and Cd(II) by phosphoric acid-modified biochars. *Environmental Pollution*, *229*, 846–853.

Rivera, F. L., Recio, F. J., Palomares, F. J., Sánchez-Marcos, J., Menéndez, N., Mazarío, E., & Herrasti, P. (2020). Fenton-like degradation enhancement of methylene blue dye with magnetic heating induction. *Journal of Electroanalytical Chemistry*, *879*, 114773.

Su, Z., Wang, K., Yang, F., & Zhuang, T. (2023). Antibiotic pollution of the Yellow River in China and its relationship with dissolved organic matter: Distribution and Source identification. *Water Research*, *235*, 119867.

Suo, F., You, X., Yin, S., Wu, H., Zhang, C., Yu, X., Sun, R., & Li, Y. (2021). Preparation and characterization of biochar derived from co-pyrolysis of Enteromorpha prolifera and corn straw and its potential as a soil amendment. *Science of The Total Environment*, *798*, 149167.

Wang, Y., Dong, X., Zang, J., Zhao, X., Jiang, F., Jiang, L., Xiong, C., Wang, N., & Fu, C. (2023). Antibiotic residues of drinking-water and its human exposure risk assessment in rural Eastern China. *Water Research*, *236*, 119940.

Watanabe, S., Tsuda, M., Terada, T., Katsura, T., & Inui, K. (2010). Reduced Renal Clearance of a Zwitterionic Substrate Cephalexin in *Mate1*-Deficient Mice. *Journal of Pharmacology and Experimental Therapeutics*, *334*(2), 651–656.

Supports

Chen, N., Zhao, T., Li, Z., Yue, X., Li, G., Zhang, J., Chen, X., Li, H., Liu, J., Xie, F., Tang, Z., Song, Y., Chen, R., Gan, J., & Li, Y. (2023). Synthesis of ternary Fe-Ca-La oxide composite as highly effective adsorbents to remove phosphate from aqueous solution. *Environmental Technology & Innovation*, *32*, 103326.

Cheng, F., Wang, Y., Fan, Y., Huang, D., Pan, J., & Li, W. (2023). Optimized Ca-Al-La modified biochar with rapid and efficient phosphate removal performance and excellent pH stability. *Arabian Journal of Chemistry*, *16*(8), 104880.

D'Cruz, B., Madkour, M., Amin, M. O., & Al-Hetlani, E. (2020). Efficient and recoverable magnetic AC-Fe$_3$O$_4$ nanocomposite for rapid removal of promazine from wastewater. *Materials Chemistry and Physics*, *240*, 122109.

Fakhri, A., & Adami, S. (2014). Adsorption and thermodynamic study of Cephalosporins antibiotics from aqueous solution onto MgO nanoparticles. *Journal of the Taiwan Institute of Chemical Engineers*, *45*(3), 1001–1006.

Fazal, T., Razzaq, A., Javed, F., Hafeez, A., Rashid, N., Amjad, U. S., Ur Rehman, M. S., Faisal, A., & Rehman, F. (2020). Integrating adsorption and photocatalysis: A cost effective strategy for textile wastewater treatment using hybrid biochar-TiO$_2$ composite. *Journal of Hazardous Materials*, *390*, 121623.

Lu, X., & Zhao, J. (2024). Adsorption of ciprofloxacin on co-pyrolyzed biochar from fish scale and pine needle. *Chinese Journal of Analytical Chemistry*, *52*(1), 100350.

Naghipour, D., Amouei, A., Estaji, M., Taghavi, K., & Allahabadi, A. (2019). Cephalexin adsorption from aqueous solutions by biochar prepared from plantain wood: equilibrium and kinetics studies. *Desalination and water treatment*, *143*, 374–381.

Rashtbari, Y., Hazrati, S., Azari, A., Afshin, S., Fazlzadeh, M., & Vosoughi, M. (2020). A novel, eco-friendly and green synthesis of PPAC-ZnO and PPAC-nZVI nanocomposite using pomegranate peel: Cephalexin adsorption experiments, mechanisms, isotherms and kinetics. *Advanced Powder Technology*, *31*(4), 1612–1623.

Viglašová, E., Galamboš, M., Diviš, D., Danková, Z., Daňo, M., Krivosudský, L., Lengauer, C. L., Matik, M., Briančin, J., & Soja, G. (2020). Engineered biochar as a tool for nitrogen pollutants removal: preparation, characterization and sorption study. *Desalination and water treatment*, *191*, 318–331.

Differences

Ali, I., T. Imanova, G., Alamri, A., Hasan, S. Z., & Basheer, A. A. (2023). Preparation of polyhydroquinone graphene oxide nanocomposite for cephalexin removal from water by adsorption: Simulation, kinetics, and thermodynamic studies. *Inorganic Chemistry Communications*, *157*, 111414.

Fan, X., Qian, Z., Liu, J., Geng, N., Hou, J., & Li, D. (2021). Investigation on the adsorption of antibiotics from water by metal loaded sewage sludge biochar. *Water Science and Technology*, *83*(3), 739–750.

Giannoulia, S., Tekerlekopoulou, A. G., & Aggelopoulos, C. A. (2024). Exploration of cephalexin adsorption mechanisms onto bauxite and palygorskite and regeneration of spent adsorbents with cold plasma bubbling. *Applied Water Science*, *14*(3), 51.

Mangeli, A., Mostafavi, A., Shamspur, T., Fathirad, F., & Mehrabi, F. (2021). Decontamination of fenitrothion from aqueous solutions using rGO/MoS$_2$/Fe$_3$O$_4$ magnetic nanosorbent: synthesis, characterization and removal application. *Journal of Environmental Health Science and Engineering*, *19*(2), 1505–1511.

Nawaz, H., Ibrahim, M., Mahmood, A., Kotchey, G. P., & Sanchez, D. V. P. (2023). An efficient synthesis and characterization of La@MOF-808: A promising strategy for effective arsenic ion removal from water. *Heliyon*, *9*(11), e21572.

Puga, A., Moreira, M. M., Pazos, M., Figueiredo, S. A., Sanromán, M. Á., Delerue-Matos, C., & Rosales, E. (2022). Continuous adsorption studies of pharmaceuticals in multicomponent mixtures by agroforestry biochar. *Journal of Environmental Chemical Engineering*, *10*(1), 106977.

Rashtbari, Y., Hazrati, S., Afshin, S., Fazlzadeh, M., & Vosoughi, M. (2018). Data on cephalexin removal using powdered activated carbon (PPAC) derived from pomegranate peel. *Data in Brief*, *20*, 1434–1439.

Wang, H.-Y., Kumar, A., Li, J., Chen, P., Yu, Z.-G., & Sun, G.-X. (2023). The adsorption behavior and mechanism for arsenate by lanthanum-loaded biochar with different modification methods. *Environmental Technology & Innovation*, *32*, 103344.

Yaghini, M., & Faghihian, H. (2020). Novel magnetized carbon core-shell impregnated with lanthanum as an adsorbent for uptake of fluoride from aquatic systems, studied by response surface methodology. *Desalination and Water Treatment*, *179*, 160–171.

Discussions

Acelas, N., Lopera, S. M., Porras, J., & Torres-Palma, R. A. (2021). Evaluating the Removal of the Antibiotic Cephalexin from Aqueous Solutions Using an Adsorbent Obtained from Palm Oil Fiber. *Molecules*, *26*(11), 3340.

Gao, Y., He, D., Wu, L., Wang, Z., Yao, Y., Huang, Z.-H., Yang, H., & Wang, M.-X. (2020). Porous and ultrafine nitrogen-doped carbon nanofibers from bacterial cellulose with superior adsorption capacity for adsorption removal of low-concentration 4-chlorophenol. *Chemical Engineering Journal*, 127411.

Groeneveld, I., Kanelli, M., Ariese, F., & van Bommel, M. R. (2023). Parameters that affect the photodegradation of dyes and pigments in solution and on substrate – An overview. *Dyes and Pigments*, *210*, 110999.

Imanipoor, J., Ghafelebashi, A., Mohammadi, M., Dinari, M., & Ehsani, M. R. (2021). Fast and effective adsorption of amoxicillin from aqueous solutions by L-methionine modified montmorillonite K10. *Colloids and Surfaces A: Physicochemical and Engineering Aspects*, *611*, 125792.

Karlsson, J. K. G., Woodford, O. J., Al-Aqar, R., & Harriman, A. (2017). Effects of Temperature and Concentration on the Rate of Photobleaching of Erythrosine in Water. *The Journal of Physical Chemistry A*, *121*(45), 8569–8576.

Kaya, N., & Uzun, Z. Y. (2024). Experimental and modeling studies on the removal of bromocresol green from aqueous solutions by using pine cone-derived activated biochar. *Biomass Conversion and Biorefinery*.

Krasucka, P., Pan, B., Sik Ok, Y., Mohan, D., Sarkar, B., & Oleszczuk, P. (2021). Engineered biochar – A sustainable solution for the removal of antibiotics from water. *Chemical Engineering Journal*, *405*, 126926.

Masulli, M., Liu, Z.-L., Guo, F.-Z., Li, X., Sudhölter, E. J. R., & Kumar, N. (2022). Temperature effect on the dynamic adsorption of anionic surfactants and alkalis to silica surfaces. *Petroleum Science*, *19*(4), 1866–1876.

Moreroa-Monyelo, M., Falayi, T., Ntuli, F., & Magwa, N. (2022). Studies towards the adsorption of sulphate ions from acid mine drainage by modified attapulgite clays. *South African Journal of Chemical Engineering*, *42*, 241–254.

Ndoun, M. C., Elliott, H. A., Preisendanz, H. E., Williams, C. F., Knopf, A., & Watson, J. E. (2021). Adsorption of pharmaceuticals from aqueous solutions using biochar derived from cotton gin waste and guayule bagasse. *Biochar*, *3*(1), 89–104.

Wernke, G., Shimabuku-Biadola, Q. L., dos Santos, T. R. T., Silva, M. F., Fagundes-Klen, M. R., & Bergamasco, R. (2020). Adsorption of cephalexin in aqueous media by graphene oxide: kinetics, isotherm, and thermodynamics. *Environmental Science and Pollution Research*, *27*(5), 4725–4736.

Wong, Y. C., Szeto, Y. S., Cheung, W. H., & McKay, G. (2008). Effect of temperature, particle size and percentage deacetylation on the adsorption of acid dyes on chitosan. *Adsorption*, *14*(1), 11–20.